WATER COLUMN CHARACTERISTICS IN THE CLARION CLIPPERTON FRACTURE ZONE, NORTH-EASTERN TROPICAL PACIFIC OCEAN

Dan VASILIU[1], Inken PREUSS[2], Mihaela MURESAN[1]

[1]National Institute for Research and Development of Marine Geology and Geoecology – GeoEcoMar), Constanta Branch, 304 Mamaia Bvd., 900581 Constanta, Romania
e-mail: dan.vasiliu@geoecomar.ro
[2]GEOMAR Helmholtz Centre For Ocean Research Kiel, 1-3 Wischhofstr., Kiel, 24148 Germany

DOI: 10.5281/zenodo.7491412

Abstract. Four exploration license areas for manganese nodules (German, Inter Ocean Metal, Belgian, and French) and one Area of Particular Environmental Interest, located within Clarion-Clipperton Fracture Zone (north-eastern tropical Pacific Ocean) were investigated in terms of CTD, nutrients and chlorophyll data during the SONNE 239 cruise carried out in March-April 2015. Chlorophyll measured either in the surface layer (concentrations within 0.05-0.15 $mg \cdot m^{-3}$) or subsurface chlorophyll maximum layer (concentrations within 0.23-0.45 $mg \cdot m^{-3}$) showed a quite low primary productivity, strongly influenced by the thermocline position. The shallow thermocline (75-90 m depth) observed in the southern edge of the studied area (≈11°N) led to a shallow and moderate subsurface chlorophyll maximum layer (50-60 m depth and concentrations within 0.4-0.45 $mg \cdot m^{-3}$). Northwards, at ≈18°N, the thermocline dropped down to 120 m depth, resulting in a deeper (110 m depth) and weaker subsurface chlorophyll maximum (concentration of 0.23 $mg \cdot m^{-3}$). The oxygen minimum layer, characteristic to the eastern Pacific Ocean, showed a spatial variability in the studied area in terms of the depth of occurrence and thickness. Thus, shallower (80-90 m depth) and thicker (thickness within 1000-1050 m) oxygen minimum zones were observed in the southernmost license areas as compared to the northernmost area (280 m depth and thickness of 750 m).

Key words: North-Eastern Pacific; Clarion-Clipperton Fracture Zone; Oxygen Minimum Zone; thermocline; chlorophyll; nutrients

1. INTRODUCTION

The abundance of deposits of polymetallic nodules in the Clarion-Clipperton Fracture Zone (CCFZ), north-eastern tropical Pacific Ocean, and their content in valuable metals (Ni, Co, Cu, Mo, Li, Ti, etc.), in addition to Mn and Fe, has resulted in an increased commercial interest during the last decades. Generally, the nodule composition shows a rather low spatial variability within CCFZ (Kuhn *et al.*, 2017), the main elements' concentrations ranging as follows: manganese = 26-30 %; iron = 5-7 %; copper = 0.98-1 %; nickel = 1-1.2 %; cobalt = 0.2 % (Tilot, 2006). The nodule abundance in the CCFZ ranges between 15 and 30 kg/m^2 (expressed as wet weight) according to the SPC (2016), thus leading to a total Mn tonnage of CCFZ nodules equals the global Mn reserves on land (ca. 6 bilion tons) and total estimated tonnages of Ni and Co (274 million tons and 44 million tons, respectively) exceeding those of land-based reserves (Visbeck and Gelpke, 2014). Consequently, many studies related to the assessment of the baseline conditions and (potential) impact of deep-sea mining on the environment, have been conducted in the area (Amos and Roels, 1977; Lavelle *et al.*, 1982, NOAA, 1981; Tkatchenko and Radziejewska, 1998; ISA, 1999; Radziejewska, 2002; Tilot, 2006; Khripounoff *et al.*, 2006).

The future deep-sea activities have will clearly impact seafloor and water column conditions and populations; however, the size of the potential impact has remained relatively difficult to assess and is still subject to many multi-disciplinary studies (Wilson and Hessler, 1987; Thiel *et al.*,

1988/1989; Hannides and Smith, 2003; Radziejewska, 2014) including the project *JPI Oceans Pilot Action – Ecological aspects of deep-sea mining (https://jpio-miningimpact.geomar.de)*.

Among other purposes (such as testing modern rapid assessment methods and monitoring techniques for defining the ecosystem status and for improving the understanding of the spatial scales and natural dynamics of abyssal environment, before and after anthropogenic disturbances in the CCFZ and DISCOL area), the above mentioned pilot action aims to investigate the background water column conditions of different areas within the CCFZ.

The eastern tropical Pacific is characterized by a moderate primary productivity, accounting for about 23% of Pacific and 10% of global oceanic primary production (Pennington *et al.* 2006). The primary productivity is strongly related to the supply of macronutrients (nitrate, phosphate) from below the thermocline (Pennington *et al.*, 2006). The main factor governing the nutrient intake into the euphotic zone in the eastern tropical Pacific is the depth of thermocline which, in turn, is controlled by a series of physical processes, all of them related to the wind regime (Wyrtki, 1966, 1967; Barber and Chavez, 1983; Pennington *et al.*, 2006). The depth of the thermocline, together with other physical processes, is also linked to one of the most important layers for the benthic communities, namely the oxygen minimum zone (OMZ).

The organic matter produced in the upper layer is subject to various transformations while sinking (degradation, decomposition, and partial dissolution) and strongly linked to the OMZ. Under certain conditions, the organic matter may sediment all the way down to the abyssal depths and reaches the seafloor as relatively undegraded phytodetritus (Billett *et al.*, 1983; Scharek *et al.*, 1999; Thiel *et al.*, 1988/1989; Radziejewska, 2014), thus contributing to diagenetic processes forming manganese nodules (Kuhn *et al.*, 2017).

Considering all these, our paper aims at studying the current conditions (hydrography, oxygen regime, nutrients and chlorophyll dynamics) in the water column in different areas within the CCFZ and providing new data/information potentially important for a better understanding of the relationship between the biological production within the upper column and that associated with the seabed. This knowledge will also help to better understand the causes responsible for different manganese nodule compositions and growth rates in the different license areas within the CCFZ.

2. MATERIAL AND METHODS

The area investigated is located within the CCFZ (North-Eastern tropical Pacific) and lies between 11°4.62′ N and 18°2.39′ N, from south to north, and 116°57.76′ W and 130°5.92′ W, from east to west (Table 1 and Fig. 1). It includes four exploration license areas (German, Inter Ocean Metal, Belgian, and French) and one Area of Particular Environmental Interest (APEI 3). The German license area (GE) was divided into 2 subareas: German Prospective Area 1 (GE-PA1) and German Reference Area (GE-RA). Inter Ocean Metal (IOM) and GE areas are located in the southeastern part of the CCFZ. Northwestward is the Belgian license area (BE), while the westernmost and northernmost are the French license area (FR) and APEI 3, respectively (Fig. 1). All these areas were investigated during the SONNE 239 – Leg 3 cruise carried out in April-May 2015 onboard RV SONNE (Table 1).

CTD equipment was deployed once in each of the six working areas in order to obtain a more complete picture of the sampled areas in terms of physical, chemical and biological conditions within the water column. Additionally, 4 CTD deployments (3 in the GE-PA1 area and 1 in the BE area) were conducted after the small scale epibenthic sledge (EBS) disturbance experiments performed in the above mentioned areas (the experiments are not discussed here). In total, 10 CTD stations were investigated, distributed as is shown in Table 1.

Vertical profiles of temperature, salinity, density (here expressed as Sigma T), dissolved oxygen (DO), and fluorescence were obtained using a SBE 911 plus CTD profiler supplied with a powerful Windows software package which includes: Seaterm, Seasave V7 (program for acquiring, converting, and displaying real-time or archived raw data), and SBE Data Processing Win32 (process the *.hex data). The raw CTD data were binned and averaged every 1 dbar from the surface to ≈ 5-10 m above the seafloor.

Criteria used for the determination of the isothermal layer (top of thermocline), isohaline layer (top of halocline) and mixed layer depths were gradients less than 0.05 °C•m-1, 0.02 PSU•m-1 and 0.01 kg•m-4, respectively, which are the same used by Lukas and Lindstrom (1991), Delcroix *et al.* (1992) and Shinoda and Lukas (1995). These criteria were applied for each cast, starting from 10 m depth for reducing the impact of the diurnal heating cycle or squalls and short duration rainfall events. The 20 °C isotherm was used for defining the depth of the thermocline (Fiedler *et al.*, 1991; Xie at al., 2005).

Water samples for nutrients and chlorophyll analyses were collected with a Sea Bird SBE 32 carrousel water sampler (24 Niskin bottles, 10L each), attached to the SBE 911 plus, from different depths selected according to the CTD vertical profiles.

Approximately 300 ml seawater were transferred to 0.5 L plastic bottles and immediately analyzed onboard for nutrients by spectrometry (UV-VIS Perkin Elmer Lambda 35 spectrophotometer) following the analytical procedures briefly described below:

- Phosphate was determined by the ascorbic acid-potassium antimony tartrate method of Murphy and Riley (1962) modified by Koroleff (2003);
- Silicate was determined by reducing (with ascorbic acid) the silicomolybdic acid formed when the sample is treated with a molybdate solution (Koroleff,1971);

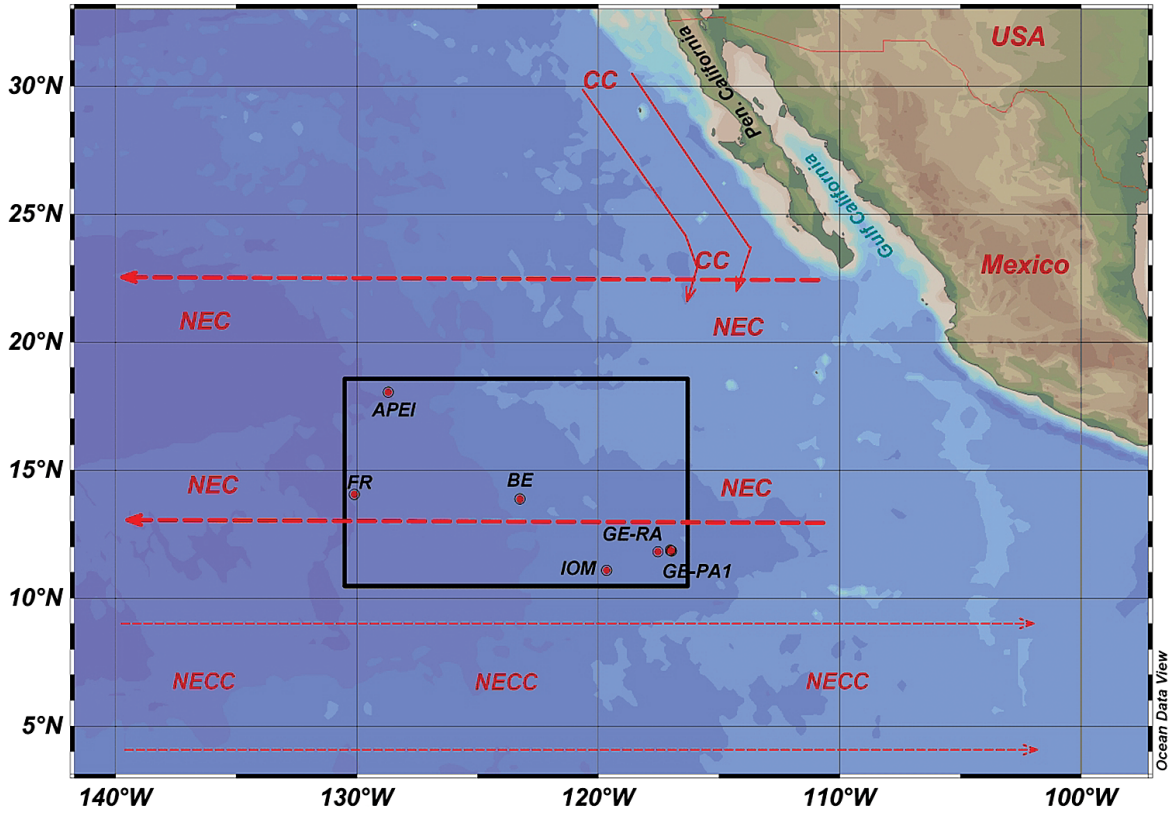

North Equatorial Current – NEC; North Equatorial Countercurrent – NECC; California Current - CC

Fig. 1. Map of studied area.

Table 1. List of CTD / rosette water sampling stations

Area	CTD stations	Coordinates	Bottom depth (m)	Samples		
German license area, prospective area (GE-PA1)	003 CTD	11°50.65′N; 116°57.77′W	4102	CTD	Nutrients	Chlorophyll
	010 CTD	11°51.53′N; 117°00.60′W	4117	CTD		
	025 CTD	11°51.31′N; 117°00.90′W	4125	CTD		
	026 CTD	11°51.63′N; 117°00.64′W	4122	CTD		
German license area, reference area (GE-RA)	056 CTD	11°48.44′N; 117°31.47′W	4366	CTD	Nutrients	Chlorophyll
Inter Ocean Metal (IOM)	074 CTD	11°04.61′N; 119°39.53′W	4432	CTD	Nutrients	Chlorophyll
Belgian license area (BE)	110 CTD	13°51.71′N; 123°14.77′W	4511	CTD	Nutrients	Chlorophyll
	118 CTD	13°52.36′N; 123°15.09′W	4512	CTD		
French license area (FR)	147 CTD	14°02.65′N; 130°05.93′W	5028	CTD	Nutrients	Chlorophyll
Area of Particular Environmental Interest (APEI 3)	183 CTD	18°2.39′N; 128°41.91′W	4768	CTD	Nutrients	Chlorophyll

- Nitrite was determined according to Bendschneider and Robinson (1952);
- Nitrate was measured based on the heterogeneous reduction to nitrite (using a cadmium-copper column) according to the method of Morris and Riley (1963) and modified by Strickland and Parssons (1968).

Seawater volumes of about 10 L were transferred from the Niskin bottles into plastic containers and filtered onboard through Millipore nitrocellulose membrane (porosity of 0.8 µm); the filters were then immediately frozen at -60 °C until the subsequent analyses (no later than 2 months). The pigments were extracted with 90 % acetone from the homogenate filter and determined by spectrometry; concentrations were calculated by using the Jeffrey and Humphrey equations (Jeffrey and Humphrey, 1975).

Differences in temperature, salinity, DO, and fluorescence (considered as the dependent variable) were established using the analysis-of-variance (ANOVA) technique and considering the working areas as fixed factors. The Tukey (HSD) test was applied to analyze the differences between every pair of groups with a confidence range of 95%. The dependent variables taken into consideration showed normal distribution (Shapiro-Wilk test) and homogeneity of variance (Bartlett test), complying with the assumptions of ANOVA.

The spatial distribution of the physical-chemical parameters in the studied area was visualized using the Ocean Data View (ODV) 4.6.2 (Schlitzer, 2014).

3. RESULTS

3.1. Hydrographic conditions

The ANOVA test followed by the multiple comparison Tukey (HSD) test revealed significant differences between the working areas in terms of temperatures in the isothermal upper layer. Significantly higher temperatures were observed in the IOM (28.02 ± 0.01 °C), followed by GE-RA (27.88 ± 0.01 °C and GE-PA1 (27.61 ± 0.01 °C) (Table 2), which lie within the westward extension of the eastern Pacific warm pool (defined by sea surface temperature greater than 27.5 °C to the east of 120 °W according to Wijesekera *et al.* (2005). Significantly lower temperatures were found in the northernmost area (APEI 3 – 23.88 ± 0.01 °C), due to the influence of the cooler waters of the California Current (CC) which feed the North Equatorial Current (NEC) at the southeastern corner of the North Pacific subtropical gyre (Fig. 1) (Kessler, 2006).

The isothermal layer depth (top of the thermocline) varied between 35 and 77 m. The thickest isothermal layer was observed in the BE area, while the thinnest one was found in the northernmost area (APEI 3) (Fig. 2).

The 20 °C isotherm depth suggests a permanent shallow thermocline in the southernmost areas (IOM and GE-RA, 74-75 m depth) (Fig. 2). The depth of thermocline increased northward, reaching a maximum of 116 m at the northernmost station 183 CTD (APEI 3). A relatively deep permanent thermocline was also observed at the westernmost station 147 CTD (FR) where the 20 °C isotherm depth was observed at 93 m.

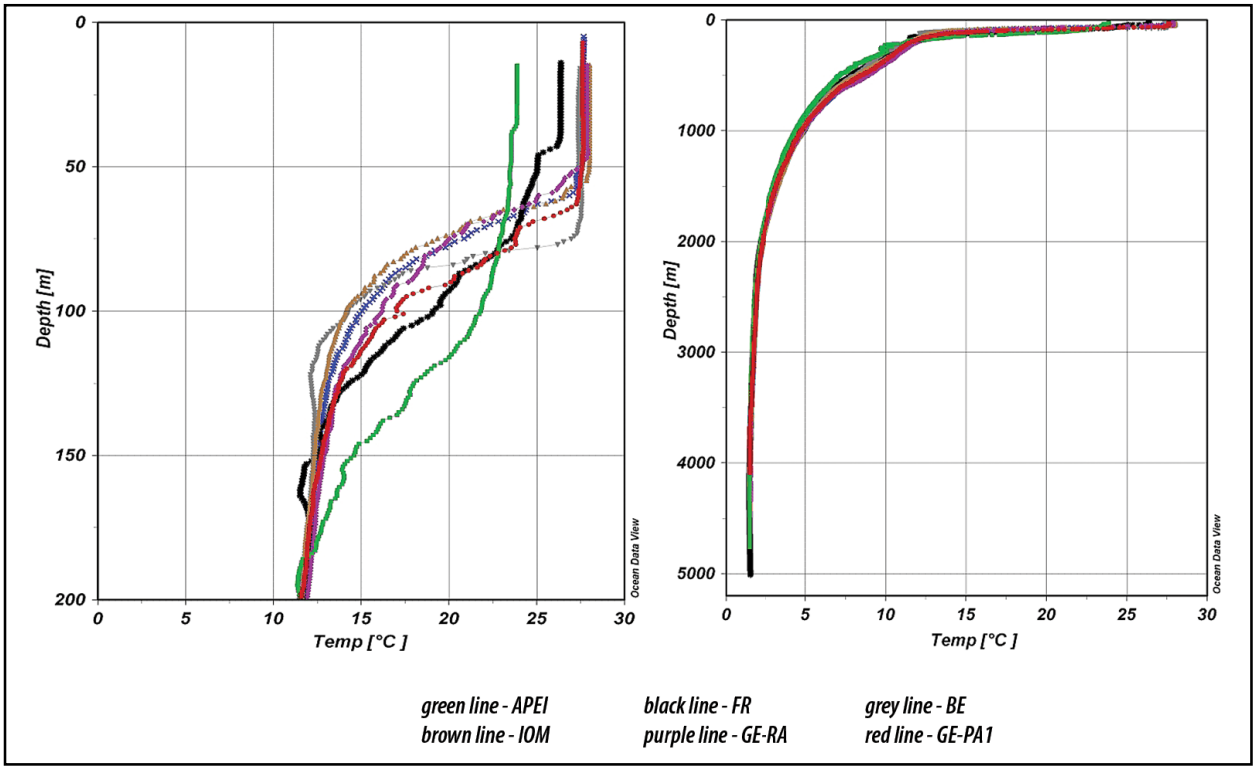

Fig. 2. Vertical profiles of seat temperature in the water column (left – upper 200 m water column; right – whole water column).

Both the FR and APEI 3 areas showed a quite thick thermocline as the isothermal depths were 42 m and 35 m, respectively. The sharpest thermocline was observed in the BE area where the 20°C isotherm depth was 84-86 m, while the top of thermocline was found at 70-77 m depth (Fig. 2).

Table 2. Sorting and grouping areas in terms of temperature, based on Tukey (HSD)/Analysis of the differences between groups with a confidence range of 95%

Areas	Mean temperature (°C)	Groupings					
IOM	28.020	A					
GE-RA	27.878		B				
GE-PA1	27.614			C			
BE	27.469				D		
FR	26.359					E	
APEI 3	23.882						F

In terms of salinity, the isohaline layer depth (top of halocline) ranged within 34-52 m, with minimum in the GE-PA1 and maximum in the GE-RA, FR and APEI 3 areas (Fig. 3). The ANOVA test followed by the multiple comparison Tukey (HSD) test revealed significant differences between the working areas in terms of salinity in the isohaline upper layer. Significantly lower salinities in the isohaline layer were found in the GE-PA1 (33.32 ± 0.07 PSU), while significantly higher ones were measured in the FR area (34.21 ± 0.02 PSU), followed by APEI 3 (34.13 ± 0.02 PSU) (Table 3). The surface salinities less than 34 PSU measured in the GE, IOM and BE areas are characteristic to the Tropical Surface Waters (Wyrtky, 1967), while those higher than 34 PSU (FR and APEI 3 areas) are related to the conversion of the less saline California Current Water into more saline Subtropical (North) Surface Water (Wyrtky, 1966).

The vertical profiles of Sigma T showed an upper mixed layer (UML) whose thickness ranged within 35-55 m. The shallowest UML was observed in the APEI 3, while the deepest one was found in the GE-PA1 (station 026 CTD). However, the mixed layer depths showed relatively low spatial variability, ranging around 40-45 m (Fig. 4).

Table 3. Sorting and grouping areas in terms of salinity, based on Tukey (HSD)/Analysis of the differences between groups with a confidence range of 95%

Areas	Mean Salinity (PSU)	Groupings				
FR	34.212	A				
APEI 3	34.128		B			
IOM	33.630			C		
GE-RA	33.627			C		
BE	33.555				D	
GE-PA1	33.352					E

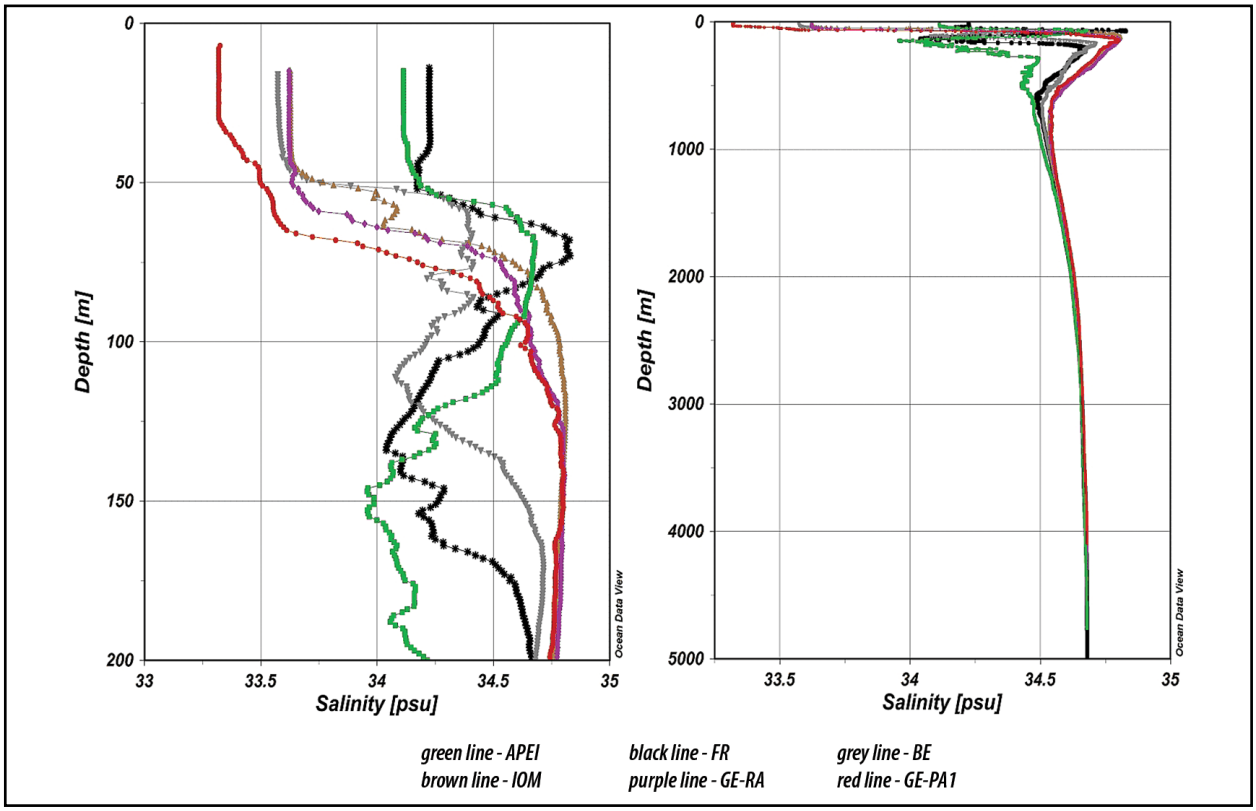

Fig. 3. Vertical profiles of salinity in the water column (left – upper 200 m water column; right – whole water column).

Beneath the UML, but within the thermocline, an alternating series of shallow salinity maxima and minima, representing cores of different subsurface water masses, as suggested by Glasby (1977) and Fiedler and Talley (2006), were observed in the BE, FR and APEI 3 areas (Fig. 3). Thus, a first maximum, showing salinities between 34.42 and 34.81 PSU (the highest value measured in the APEI 3) was observed at depths of 70-80 m. According to Wyrtki (1967), this shallow salinity maximum layer is associated with Subtropical Subsurface (North) Water formed in the North Pacific subtropical gyre. Beneath it, a shallow salinity minimum (34.0-34.1 PSU), originating in the California Current (Reid, 1973), can be observed at 100-150 m depth (Fig. 3). These salinity maximum and minimum layers were not observed in the IOM and GE areas.

At the lower thermocline, a deep salinity maximum, corresponding to the Subtropical Subsurface (South) Water, was observed in all sampling stations (Fig. 4). The GE and IOM areas showed the salinity maximum (34.80-34.81 PSU) at depths of 135-160 m and 115-135 m, respectively. The lower portion of the deep salinity maximum layer spread northward where it met the California Current, leading to the deepening of the lower salinity maximum to 200-210 m in the FR area (34.67 PSU) and 285-295 m in the APEI 3 area (34.5 PSU), in accordance with Wyrtki (1967).

Between 500 and 900 m depth a low salinity Intermediate Water mass separates the subsurface waters from deeper waters. It is associated with the deep salinity minimum and seems to originate from two sources, according to Fiedler and Talley (2006): i) the Antarctic Intermediate Water (AIW), formed from the deep, winter mixed layer north of the Subantarctic Front in the southeast Pacific (Hanawa and Talley, 2001) spreading equatorward and westward in the Pacific and ii) the North Pacific Intermediate Water (NPIW), which originates from subsidence in the Sea of Okhotsk and at the Oyashio Front in the western North Pacific, with some contribution from the Gulf of Alaska (You, 2003). The APEI 3 showed a deep salinity minimum (34.44 PSU) at depths of 510-540 m, which is characteristic to the NPIW, thus showing a less prominent signature of the AIW (Glasby, 1977; Fiedler and Talley, 2006). On contrary, the AIW seems to play a more important role in the southernmost areas, which results in the deepening of the salinity minimum layer (750-900 m) and higher concentrations in its core (34.53-34.54 PSU) (Fig. 4).

The temperatures gently decrease within the low salinity Intermediate Water from 7.15-8.9 °C (minimum in the APEI 3, maximum in the GE-RA) to 4.4-4.9 °C (minimum in the APEI 3, maximum in the GE-PA1).

The deep water (DW) between 1000 and 2500 m is characterized by a gentle decrease in temperature (from 4.40-4.89 °C to 1.78-1.90 °C) and an increase in salinity (from 34.51-34.55 PSU to 34.64-34.65 PSU). The lower limits were observed in the northernmost area (APEI 3), whereas the upper ones in the southernmost areas (Figs. 2 and 3). Deeper than 2500 m, the North Pacific Deep Water (NPDW), characterized by temperatures within 1.46-1.90 °C and salinities within 34.65-34.68 PSU, is overlying the near bottom water (bottom depths > 4000 m).

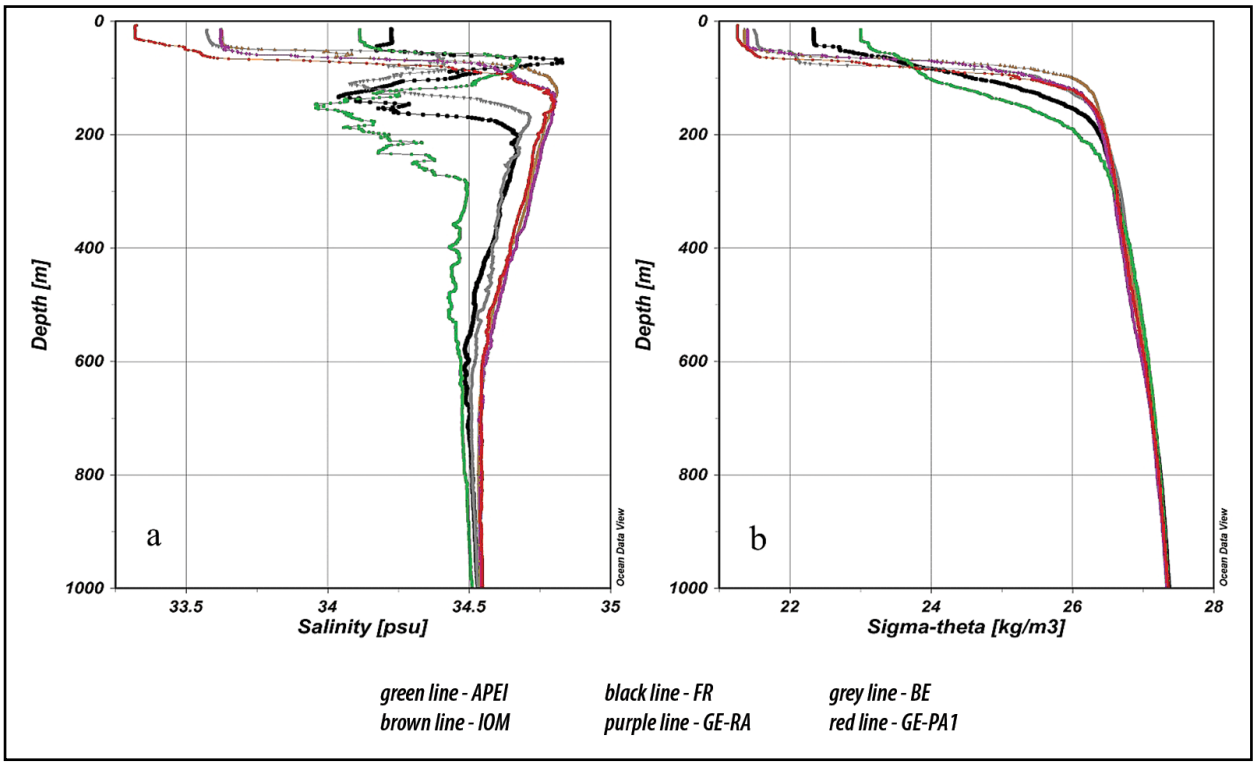

Fig. 4. Vertical profiles of salinity (left) and Sig T (right) in the upper 1000 m water column.

The latter, characterized by temperatures within 1.48-1.50 °C and salinity of 34.68 PSU (Figs. 2 and 3), is formed by the Lower Circumpolar Water (LCPW), a mixture of Antarctic Bottom Water (AABW) and the North Atlantic Deep Water (NADW) formed in the northern North Atlantic (Fiedler and Talley, 2006).

3.2. Dissolved Oxygen (DO)

DO concentrations and saturation in the UML varied between 4.13 and 4.52 ml·L^{-1}, and 90.42 % and 93.86 %, respectively, thus suggesting a quite well oxygenation of the surface water. The ANOVA test followed by the multiple comparison Tukey (HSD) test revealed significant differences between the working areas in terms of DO concentration and saturation. Significantly lower DO concentrations and saturations were found in the IOM area (4.16 ± 0.02 ml·L^{-1} and 91.68 % ± 0.34 %, respectively) (Tables 4 and 5). As regarding the DO concentrations, significantly higher values were measured in the APEI 3 (4.51 ± 0.01 ml·L^{-1}), followed by the FR and BE areas (4.29 ± 0.01 ml·L^{-1} and 4.24 ± 0.02 ml·L^{-1}, respectively) (Table 4). DO saturation showed no significant differences between APEI 3, FR and BE areas (Table 5).

DO vertical profiles showed a sharp oxycline at the southernmost stations (IOM and GE areas) from around the upper limit of the thermocline (46-56 m) down to 85-110 m, where DO dropped below 0.1 ml·L^{-1} (Fig. 5). The upper limit of the oxycline descended northwards to 73-80 m in the BE area and ≈120 m in the APEI 3.

Table 4. Sorting and grouping areas in terms of DO concentration based on Tukey/(HSD)/Analysis of the differences between groups with a confidence range of 95%

Areas	Mean DO (ml·L^{-1})	Groupings					
APEI 3	4.506	A					
FR	4.298		B				
BE	4.242			C			
GE-PA1	4.219				D		
GE-RA	4.193					E	
IOM	4.162						F

Table 5. Sorting and grouping areas in terms of DO saturation based on Tukey/(HSD)/Analysis of the differences between groups with a confidence range of 95%

Areas	Mean DO (%)	Groupings		
APEI 3	92.804	A		
BE	92.694	A		
FR	92.405	A	B	
GE-PA1	92.176		B	
GE-RA	92.121		B	
IOM	91.682			C

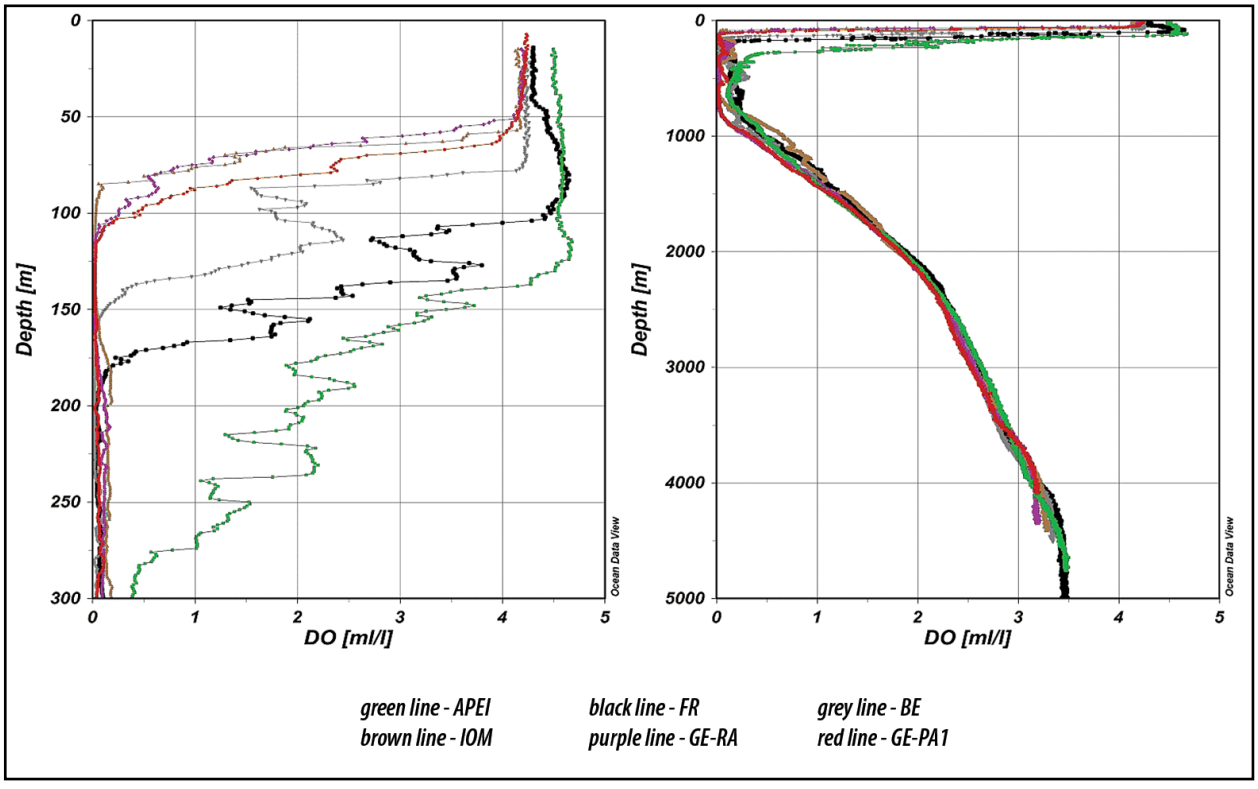

Fig. 5. Vertical profiles of dissolved oxygen concentration in the water column (left – upper 300 m water column; right – whole water column).

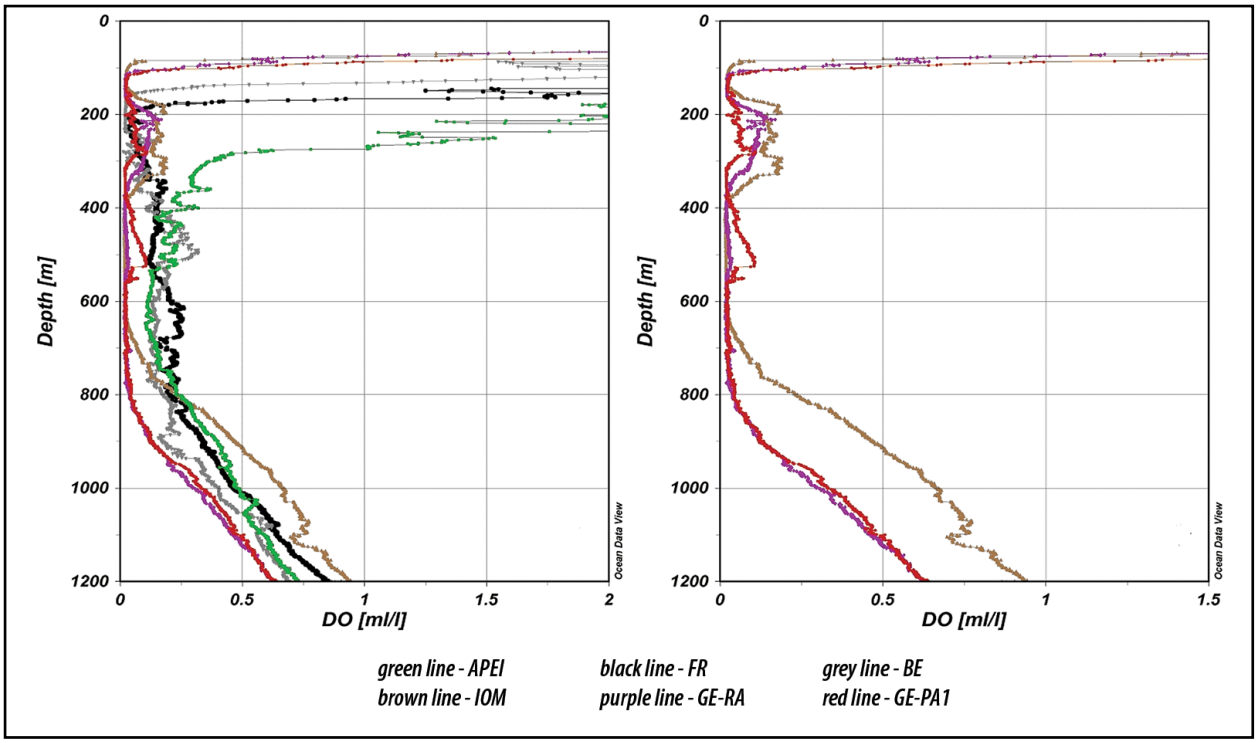

Fig. 6. Vertical profiles of dissolved oxygen concentration in the upper 1200 m water column.

In these areas the oxycline was interrupted by an increase in DO up to 2.4-3.8 ml·L^{-1} at depths corresponding to the shallow salinity minimum layer (110-150 m), most likely in connection with the cooler, less saline and more oxygenated waters of California Current. The thickness of the oxycline increased significantly northwards, from ≈30 m in the IOM area to 70-75 m in the BE area and ≈170 m in the APEI 3 (Fig. 5).

Beneath the oxycline, the Oxygen Minimum Zone (OMZ) encompasses the depth range of 80-1140 m (Figs. 5 and 6). The upper and lower limits of OMZ are here considered the depths corresponding to DO concentration of 0.5 ml·L^{-1} (≈22 μM·L^{-1}), according to Levin (2003).

The thickness of the OMZ decreased from ≈1050 m in the southeastern part of the studied area (GE area) to ≈750 m in the northwestern part (APEI 3). The shallowest OMZ was found in the southern areas (upper limit below 100 m), while the deepest one was observed in the APEI 3 (upper limit at ≈280 m) (Fig. 6).

The minimal DO concentrations were around 0.02 ml·L^{-1}, except the APEI 3 (minimum of 0.11 ml·L^{-1}) where the less sharp pycnocline (Fig. 4) allows a slight vertical ventilation. The core of the OMZ (here considered between the depths corresponding to 0.1 ml·L^{-1} or 4.5 μM·L^{-1}) was observed between depths of 85 m and 880 m. Thicker and shallower cores of the OMZ were found in the south of the studied area (750-770 m and 85-105 m, respectively) (Fig. 6). The thickness of the OMZ core significantly decreased northwestward to 270 m and 150 m in the BE and FR areas, respectively, whereas the depth of occurrence descended to 150 m and 180 m in the BE and FR areas, respectively. In the APEI area, a relatively thin layer with DO concentrations close to 0.1 ml·L^{-1} was observed between depths of 600 m and 660 m. The lower OMZ boundary exhibited a more gradual increase in oxygen with water depth.

Beneath the OMZ, the DO concentrations showed a less steep increase down to near bottom waters, where its concentrations reached values within 3.18-3.49 ml·L^{-1} (Fig. 5), significantly higher than the level of 2 ml·L^{-1} which is considered the critical threshold for the survival of benthic communities (Rabalais *et al.*, 2010). The highest near bottom DO concentrations were found in the FR and APEI 3 areas (3.45-3.49 ml·L^{-1}), where also the DO saturations in the bottom waters were maximal (44.9-45.0 %).

3.3. Nutrients

Nutrients showed relatively low concentrations in the UML, ranging within 0.09-0.37 μM for PO_4; 0.23-0.96 μM for SiO_4; 0.09-0.60 μM for NO_3. Surface nitrite showed concentrations below the detection limit (0.003 μM).

Surface phosphate showed the highest concentration in the APEI 3, followed by FR area (0.19 μM), while the lowest one was measured in the IOM area. Silicate showed the maximal concentration in the FR area and the minimal one in the APEI 3. Nitrate showed a relatively homogeneous distribution in the thin surface layer (minimum of 0.10 μM in the GE-PA1 and maximum of 0.27 μM in the BE area).

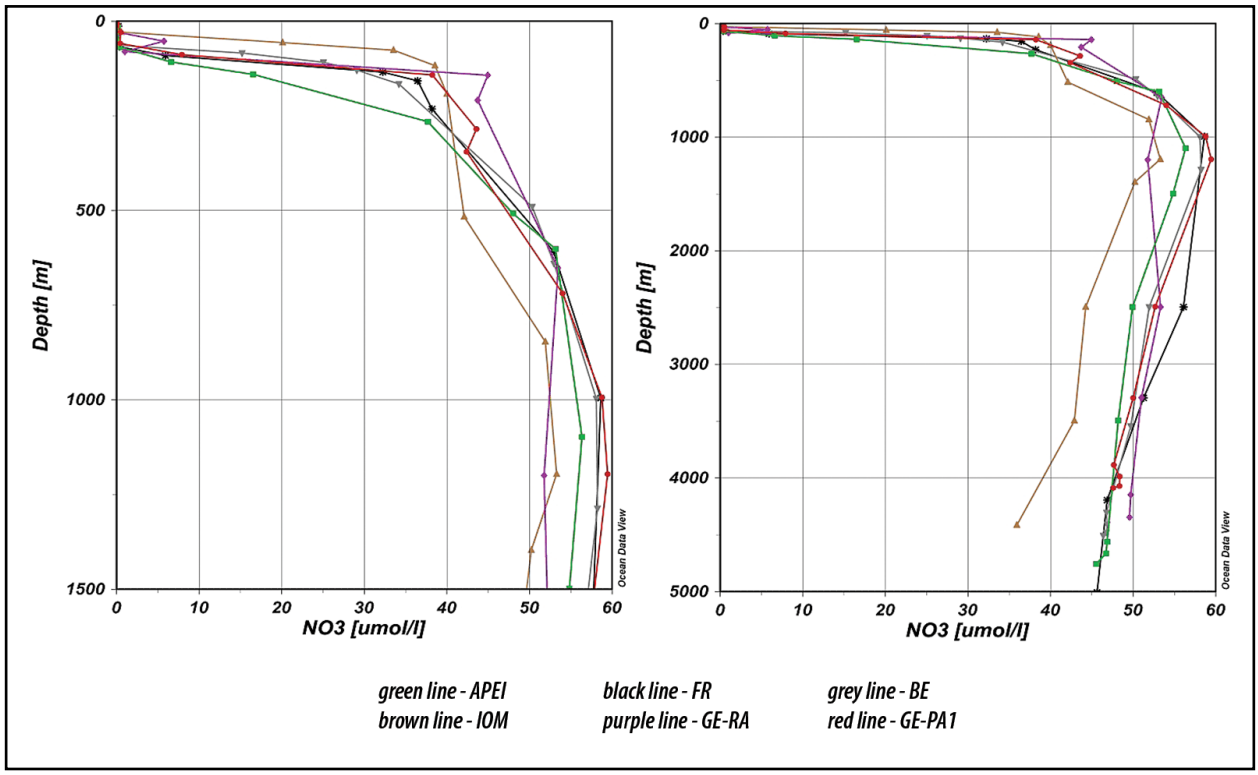

Fig. 7. Vertical profiles of nitrate in the water column (left – upper 1500 m water column; right – whole water column).

A slight increase in nitrate concentration was observed at the lower boundary of UML, but the concentrations remained below 1 µM. Unlike nitrate, either phosphate or silicate did not show significant differences within the UML. However, the surface nutrient concentrations measured during the cruise are consistent with those provided by Fiedler and Talley (2006).

An increase in nutrient stock was observed in the GE, IOM and BE areas, just below the upper limit of the thermocline (Figs. 7, 8, 9, and 10), thus suggesting the top of nutricline at around the isothermal depth (≈50 – 75 m depth).

In the FR and APEI 3 areas, the top of the nutricline seems to be situated significantly below the isothermal layer depth since the nitrate concentrations at 68-69 m depth did not differ greatly from those recorded in the isothermal layer (0.39 µM as compared to 0.15-0.23 µM) (Fig. 7). This could be related to the less steep upper part of the thermocline, followed by a sharper part which limits the nutrient upward transport (Fig. 2). Anyhow, the top of the nutricline / nitracline seems to be situated at depth of ≈80 m since the nitrate concentrations found at the depth corresponding to the deep chlorophyll maximum (DCM) layer (90-110 m) were significantly higher (5.95 µM and 6.62 µM in the FR and APEI 3 areas, respectively) (Fig. 7). Nitrite showed a maximum (0.02-1.16 µM) at depths corresponding to the DCM layer (Fig. 8), most likely associated with the excretion by phytoplankton (Vaccaro and Ryther, 1960) and/or nitrification of ammonium by chemoautotrophic bacteria (Dore and Karl, 1996).

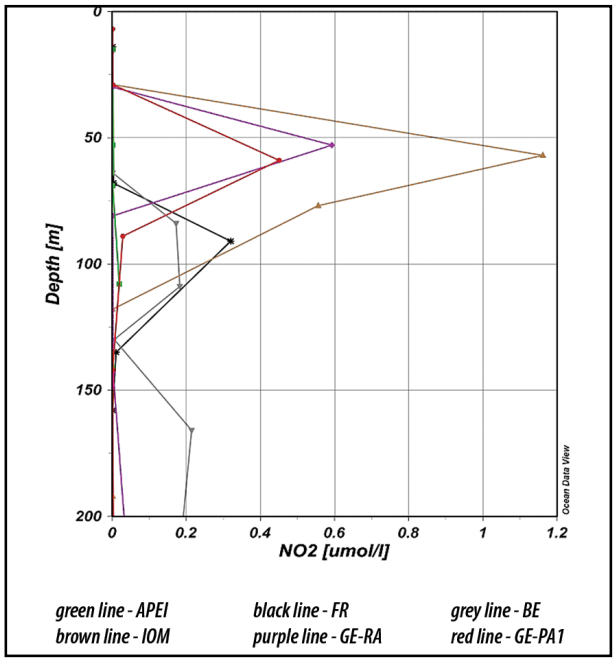

Fig. 8. Vertical profiles of nitrite in the upper 200 m water column.

A sharp upper part of the nutricline/nitracline was observed within the oxycline (down to the upper part of the OMZ), where the oxidizing decomposition of organic matter led to a nutrient sharp increase. The nutrient concentrations around the upper limit of the OMZ ranged within 34.22-44.98 µM for NO_3, 2.01-2.59 µM for PO_4, and 13.65-20.67 µM for SiO_4.

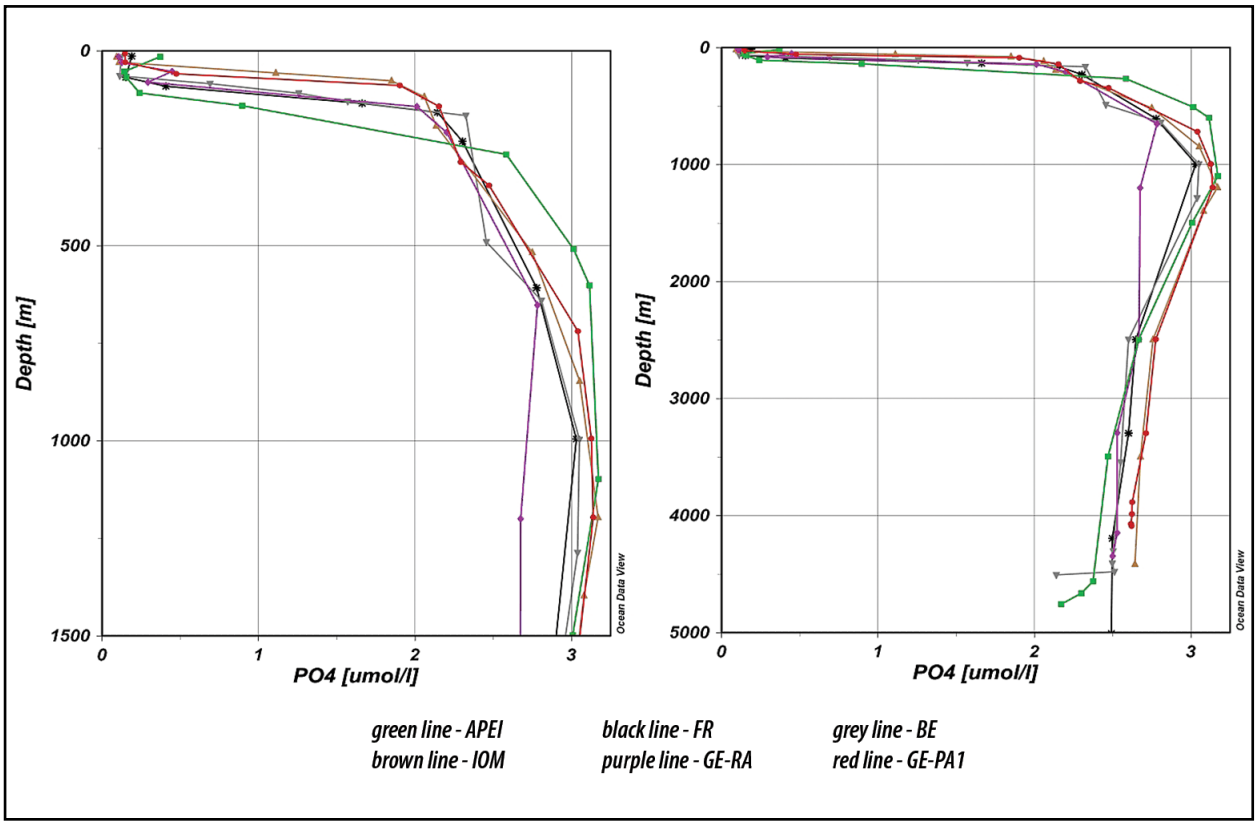

Fig. 9. Vertical profiles of silicate in the water column (left – upper 1500 m water column; right – whole water column).

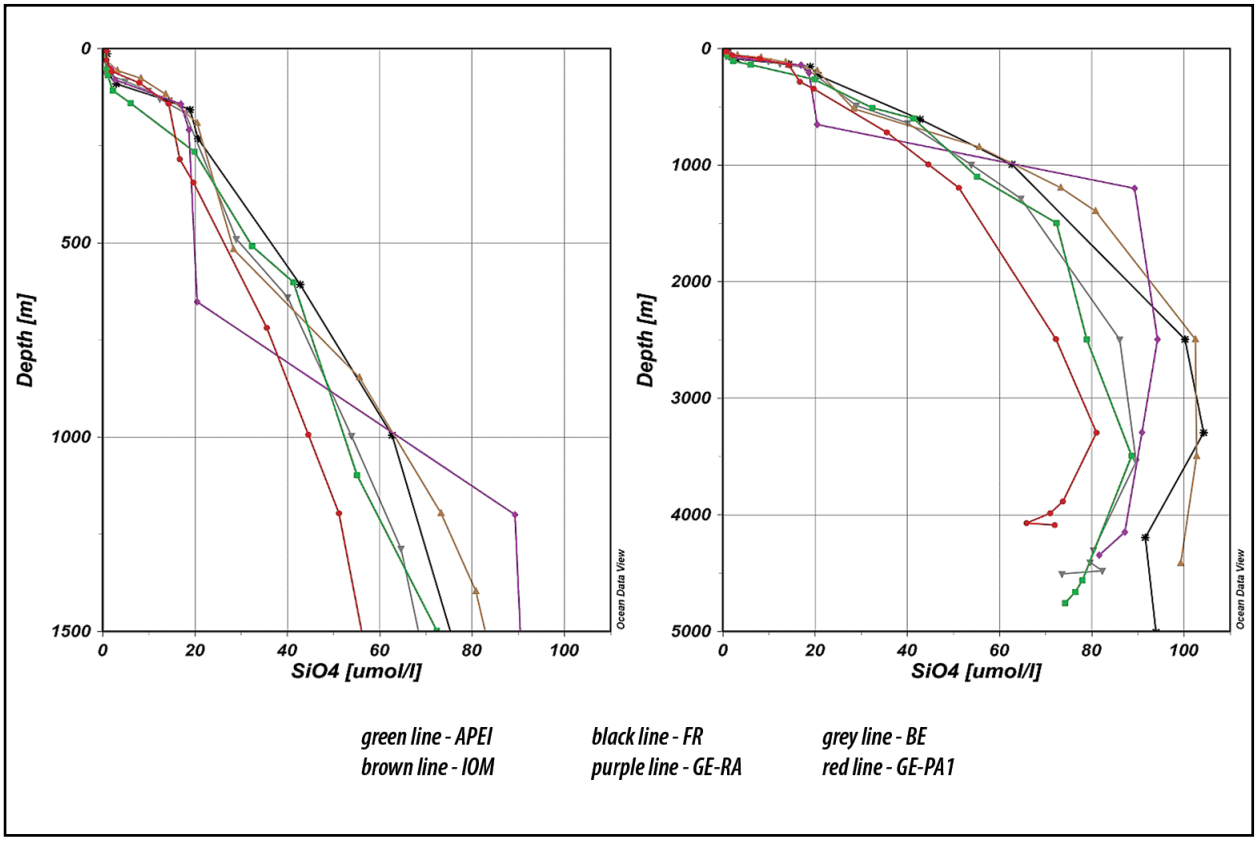

Fig. 10. Vertical profiles of phosphate in the water column (left – upper 1500 m water column; right – whole water column).

Higher nitrate and lower phosphate concentrations at the upper boundary of the OMZ were found in the southernmost stations (Figs. 7, 9, and 10).

Nitrate showed a less steep increase within the OMZ (especially at the southernmost stations) reaching a maximum at around the lower limit of the OMZ (1000-1200 m depth). The maximal concentrations ranged within 53.30-59.48 µM, both extremes being observed in the GE areas (Fig. 7). Phosphate showed a similar pattern, the maximal concentrations of 2.78-3.17 µM were observed at the same depths (higher concentrations in the IOM and APEI 3 areas) (Fig. 9). Both phosphate and nitrate maxima corresponded to the Intermediate Water salinity minimum. Unlike nitrate and phosphate, the silicate showed a relatively sharp increase within the OMZ, reaching concentrations of 17-89.31 µM at the lower boundary of the OMZ. The concentrations increased steadily up to maximal values, ranging from 81.07 µM (GE-PA1) to 104.25 µM (FR area), measured within NPDW, at depths within 2500-3500 m (both extreme concentrations were recorded at 3300 m depth) (Fig. 10).

For some of the stations (056 CTD, 110 CTD, 147 CTD, and 183 CTD) a secondary nitrite maximum (much weaker than the shallower one – 0.03-0.21 µM, with maximum at station 110 CTD) was observed within the upper part of the OMZ (Fig. 8). This second nitrite maximum appears to be associated with the DO concentrations less than 0.1 ml/l and suggests anaerobic nitrate reduction (Brandhorst, 1959).

Beneath the nutricline, nutrient concentrations showed a slight decrease down towards near bottom waters, where they reached concentrations ranging within 2.04-2.64 µM for PO_4; 35.37-49.72 µM for NO_3; and 60.66-99.29 µM for SiO_4 (Figs. 7, 9, and 10).

3.4. CTD fluorescence and chlorophyll

The ANOVA test followed by multiple comparison Tukey (HSD) test revealed significant differences between the areas in terms of CTD fluorescence in the UML. The highest values were observed in the southernmost areas (GE-RA – 0.35 ± 0.01 mg·m^{-3}; IOM – 0.11 ± 0.03 mg/m^3; and GE-PA1 – 0.09 ± 0.04 mg/m^3), while the lowest ones were measured in the northernmost and westernmost areas (APEI 3 and FR areas with 0.03 ± 0.03 mg·m^{-3} and 0.05 ± 0.04 mg·m^{-3}, respectively) (Table 6).

Surface chlorophyll *a* concentrations showed a similar spatial distribution with maximum in the GE-RA (0.15 mg·m^{-3}) and minima in the APEI 3 and FR areas (0.07 ± 0.02 mg·m^{-3} and 0.09 mg·m^{-3}, respectively).

The CTD data revealed a fluorescence maximum layer at depths ranging from 52 to 113 m. Shallower fluorescence maxima were found in the southernmost areas, with the upper boundary between 52 m and 58 m depth (Fig. 11), generally just below the upper limit of the thermocline. The fluorescence maximum layer descended northwards; the deepest maxima were observed in the APEI 3 and FR areas (upper limits at depths of 90 m and 107 m, respectively). The core of the fluorescence maximum layer was found at 53-65 m depth in the GE and IOM areas, 82-90 m depth in the BE area, 93 m depth in the FR area, and 112 m depth in the APEI 3 (Fig. 11). The highest fluorescence values were found in the GE-PA1, particularly at the stations 025 CTD (1.46 mg·m^{-3}) and 026 CTD (1.51 mg·m^{-3}), but high concentrations were measured in the BE area (1.31-1.35 mg·m^{-3}) as well. The weakest fluorescence maxima were measured in the APEI 3 and FR areas (0.63 mg·m^{-3} and 0.86 mg·m^{-3}, respectively) (Fig. 11).

Table 6. Sorting and grouping areas in terms of surface fluorescence based on Tukey (HSD)/Analysis of the differences between groups with a confidence range of 95%

Areas	Mean fluorescence (mg·m^{-3})	Groupings				
GE-RA	0.354	A				
IOM	0.111		B			
GE-PA1	0.090		B	C		
BE	0.076			C		
FR	0.053				D	
APEI 3	0.031					E

The chlorophyll *a* data showed a similar downward profile. Thus, the deep chlorophyll maximum (DCM) layer was found approximately at the same depths with the fluorescence maximum. Nevertheless, the chlorophyll concentrations measured in the DCM layer (0.23-0.45 mg·m^{-3}) were significantly lower than the CTD fluorescence. The chlorophyll concentrations in the DCM core showed the lowest values in the APEI 3 and FR areas (0.23 and 0.24 mg·m^{-3}, respectively). The highest concentrations were observed in the southern areas (GE-PA1 and IOM areas with 0.45 and 0.44 mg·m^{-3}, respectively), in connection with the shallower DCM (Fig. 11). This is in accordance with the significant negative correlation found between the DCM depth and the chlorophyll concentration of the maximum layer (r= -0.869, p=0.024).

The southernmost stations showed also a second subsurface fluorescence maximum at depths corresponding to the deep salinity maximum layer (90-146 m), in the upper part of the OMZ. These maxima are less pronounced than the shallower ones, the fluorescence varying between 0.41 mg·m^{-3} and 0.98 mg·m^{-3} (Fig.11)

The presence of the second fluorescence maximum is associated with shallower OMZ, where the upper limit of the OMZ overlaps the euphotic depth (Cepeda – Morales *et al.*, 2009). Thus, the strongest and shallowest second fluorescence maximum was observed in the IOM area, where the OMZ upper limit was shallower.

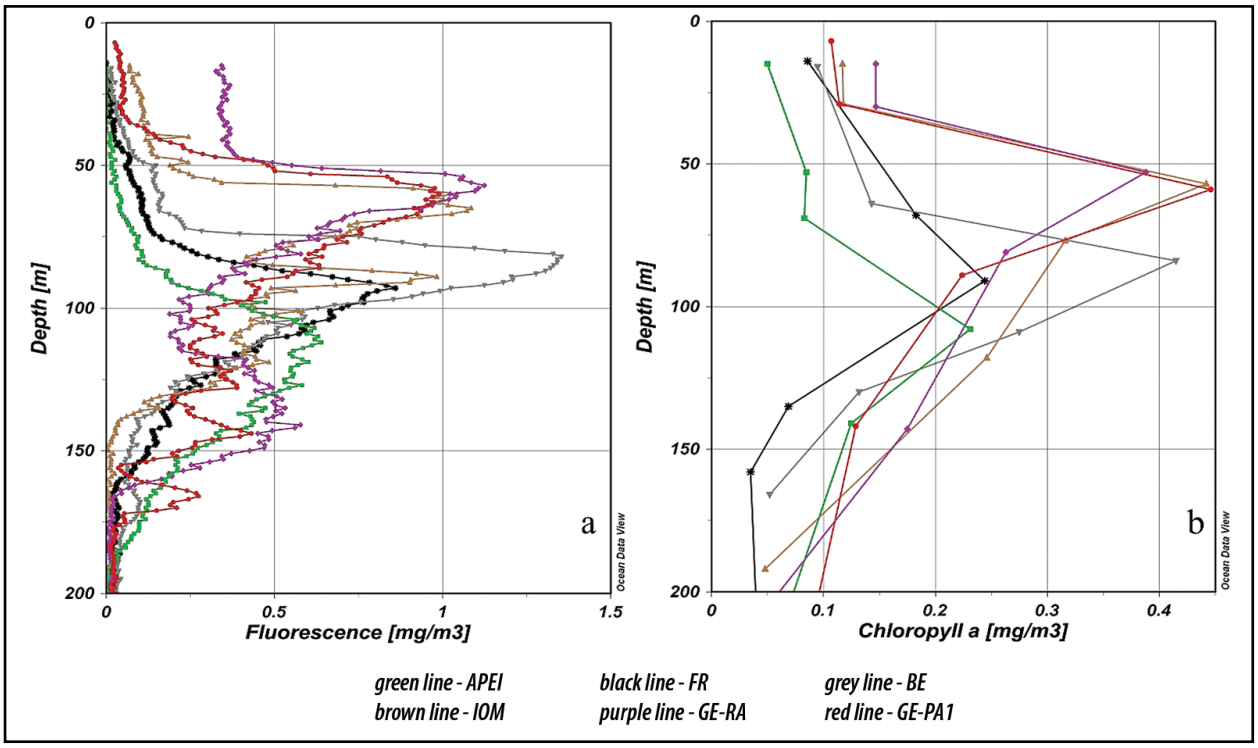

Fig. 11. Vertical profiles of CTD fluorescence (left) and chlorophyll a (right) in the upper 200 m water column.

The deepening of the upper limit of the OMZ led to the weakening or absence of the second fluorescence maximum. Thus, in the BE area, a very weak (0.10-0.11 mg·m^{-3}) deeper fluorescence maximum (165-170 m) was observed, while in the FR and APEI 3 areas this maximum was completely absent (Fig. 11).

Unfortunately, the chlorophyll *a* profiles did not show the second maximum due to the small number of samples collected. Mostly, only one sample was collected between the DCM depth and the depths corresponding to the second fluorescence maximum *per* station, chlorophyll *a* showing concentrations within 0.12-0.25 mg·m^{-3}).

4. DISCUSSIONS AND CONCLUSIONS

This section aims at emphasizing the relationships among the thermohaline structure of the water column, the productive part of the water column and the OMZ layer, with significant impact on the biodiversity/bioproductivity either within the water column or on the seafloor.

The studied area is situated within the North Equatorial Current (NEC), flowing westward under the influence of the N/NE trade winds. Southward, at about 10ºN, there is the North Equatorial Countercurrent (NECC) which flows eastward, thus in opposition to NEC (Fig. 1). Between these currents, there is a region of thermocline shoaling which is caused by positive wind stress curl cross the Intertropical Convergence Zone (ITCZ) and termed countercurrent thermocline ridge by Fiedler and Talley (2006).

The southernmost sampling areas (IOM and GE) are linked to this zonal feature, the 20°C isotherm depths observed there showing shallower thermocline. The relatively low number of nutrient data collected during the investigated period makes quite difficult to point out the actual depth of the top of nutricline/nitracline (relative to the top of thermocline). However, our data suggested a shallow and sharp nutricline in the IOM and GE areas, in accordance with Pennington *et al.* (2006) observations, thus leading to an increased nutrient stock within the euphotic zone. The surface chlorophyll concentrations measured in the IOM and GE areas (0.11-0.15 mg·m^{-3}) are in agreement with data provided by Pennington *et al.* (2006) for the countercurrent thermocline ridge region (surface chlorophyll concentration of 0.14 mg·m^{-3}). Close to the top of the nutricline, the CTD fluorescence data showed a quite pronounced DCM layer for this region. The chlorophyll concentrations in the DCM layer (0.40-0.45 mg·m^{-3}) were found to be higher in our study as compared with the values provided by Pennington *et al.* (2006) (between 0.2 mg·m^{-3} and 0.3 mg·m^{-3}).

The 20° isotherm showed a deepening of the thermocline from 70-75 m to 85-95 m in the BE and FR areas, at ≈14 °N, north of countercurrent thermocline ridge. The difference between these areas in terms of the thermocline position is given by the depth of the top of the thermocline. A significantly shallower top of the thermocline was observed westwards (in the FR area, ≈130°W), thus a thicker thermocline which led to smaller chlorophyll concentrations (Table 6) and, most likely, lower primary productivity in the surface layer.

APEI 3, the northernmost studied area (at ≈18°N) showed the deepest 20°C isotherm (at 115 m depth) and thickest thermocline, which is associated with a chlorophyll upper layer. The average chlorophyll concentration in the upper layer was 0.092 mg·m^{-3}, similar to the data provided by Fiedler and Talley (2006) and Pennington *et al.* (2006) for the NEC region (0.09 mg·m^{-3}). The NEC surface chlorophyll measured either at 14°N (0.09 mg·m^{-3}) or 18°N showed lower concentrations than in the countercurrent thermocline ridge region, in accordance with the Pennington *et al.* (2006) observations. This northward decrease of surface chlorophyll is also strongly supported by the significant negative correlation found between the 20°C isotherm depth and the surface chlorophyll (r= -0.913, p=0.011). However, all these observations suggest a quite low productive upper mixed layer in the CCFZ, in line with the satellite observations-based (SeaWiFS; http://seawifs.gsfc.nasa.gov) and ship-based data on chlorophyll *a* distribution in the CCFZ (Morgan, 2000; Pennington *et al.*, 2006).

The DCM layer in the NEC region was found deeper as compared to countercurrent thermocline ridge region. Contrary to the southern studied areas, where the DCM was found at the upper limit of the thermocline, in the BE and FR areas it was observed at around 20°C isotherm depth, thus approximately at the center of the thermocline. This seems to be related to the alternating of the shallow salinity maximum and minimum layers, which acts on the pycnocline shape/thickness, thus on the nutrient vertical transport and, consequently, primary productivity in the euphotic zone. More pronounced upper salinity maximum and minimum (leading to a thicker pycnocline) observed in the FR area led to a weaker subsurface chlorophyll maximum, thus suggesting a decrease in the DCM magnitude (chlorophyll concentrations in the DCM core) westward. This is linked to the nutrient concentrations measured at the DCM depth, which showed significant lower concentrations (particularly the nitrate) in the FR area (5.95 µM) as compared to the BE area (15.21 µM).

The DCM depth of 80-90 m found at 14°N was in accordance with Pennington *et al.* (2006) who observed that DCM depth for the NEC region is fairly constant at ≈ 80 m. Unlike the Pennington *et al.* (2006) observations, the DCM depth observed at 18°N (in the APEI 3) was deeper than 100 m. However, comparing the shape and magnitude of the DCM, it can be observed that the APEI 3 showed the thickest DCM, but with the lowest chlorophyll concentrations (Fig. 11). The nutrient concentrations measured at 20°C isotherm depth showed values quite close to those recorded in the westernmost area (FR), thus suggesting the influence of the nutrient depleted Subtropical North Pacific gyre (reference).

Summarizing, the thermocline topography in the studied area plays a major role in regulating the primary productivity in the productive upper column. The deepening of the permanent thermocline northwards is associated with the lower surface chlorophyll and deeper and weaker DCM, thus suggesting a decrease in the primary productivity, which is in line with the previous studies (Fiedler *et al.*, 1991; Fiedler and Talley, 2006; Pennington *et al.*, 2006).

The hydrography of the investigated region plays also a major role in terms of OMZ spatial variability and its characteristics. The OMZ was observed throughout the entire studied area, even if its shape and DO concentrations in its core showed a spatial variability. The depth of occurrence of the OMZ showed a northward decrease. The shallowest OMZ was observed in the southern areas (GE and IOM), while the deepest one was found in the northernmost area (APEI 3). This is in agreement with the significant positive correlation (r=0.918, p<0.0001) found between the depths of the 20°C isotherm and the OMZ upper boundary, thus suggesting the deepening of the upper limit of the OMZ northwards, where the thermocline is deeper.

In terms of OMZ thickness, no significant relationship was found with the 20°C isotherm depth. Thus, the decrease of OMZ thickness northwards seems not to be related to the thermocline deepening, but rather to the OMZ shape. The OMZ thickness is larger in the southernmost areas, where two DO minima/cores (≈0.02 ml·L^{-1}) were observed (Fig. 6). These two minima are separated by a slight increase in DO (up to 0.14-0.18 ml·L^{-1}), which is, most likely, due to the influx of western water borne by Equatorial Underwater Current (EUC), according to Wyrtki (1967). The shallower DO minimum is associated with salinities within 34.68-34.81 PSU that correspond to the values of the deep salinity maximum in the core of the Subtropical Subsurface Waters (Fiedler and Talley, 2006). The deeper DO minimum followed the deep salinity minimum and was associated with constant salinities at around 34.55 PSU, characteristic to the Intermediate Water (Fiedler and Talley, 2006).

The decrease of the OMZ thickness towards north is associated with the change in its shape, specifically with the presence of only one DO minimum (the shallower one). Therefore, at ≈14°N, a shallow OMZ core was observed at the salinity maximum depth as well (34.67-34.71 PSU; Fig. 6), but no deeper OMZ core was found at depths corresponding to deep salinity minimum. Here, DO showed concentrations (0.18-0.25 ml·L^{-1}) higher than 0.1 ml·L^{-1}, which is considered the OMZ core boundary. However, the concentrations found at depths corresponding to deep salinity minimum were higher in the FR area (≈130°W), suggesting a weakness of the OMZ towards west, which is in accordance with previous observations (Zheng *et al.*, 2000). At ≈18°N, the DO concentration showed the minimum of 0.11 ml·L^{-1} at the lower boundary of the deep salinity minimum (corresponding to NPIW), contrary to the FR and BE areas. The deepening of the OMZ core down to depths corresponding to the NPIW (500-700 m) in the APEI 3 can be linked to the less sharp pycnocline in this area (Fig. 4b), resulted from an increase in vertical ventilation.

Hence, the GE and IOM areas (lying within the westward extension of the eastern Pacific warm pool) showed more pronounced oxygen depletion in the subpycnocline waters. This is in accordance with Fiedler and Talley (2006) who showed that the greatest depletion below the strong pycnocline is characteristic for the eastern Pacific warm pool, where the ventilation by intermediate water through a long and convoluted path is low and the biological productivity is higher. Northwards, the lower productivity in the upper layer, the increased ventilation due to less sharp pycnocline and the shallower position of the deep salinity minimum led to a decrease in the thickness and intensity of the OMZ, which is in accordance with Zheng *et al.* (2000).

At the upper limit of the OMZ, a quite well pronounced secondary chlorophyll maximum was found in the southern areas (within the countercurrent thermocline ridge region) (Fig. 11a). It appears to be linked to the more saline subsurface waters (≥ 38 PSU) (Odate and Furuya, 1998), characteristic to the Subtropical Subsurface (South) Water, which originates in South Pacific Subtropical Gyre and penetrates across the Equator to the northern hemisphere. Pennington *et al.* (2006) suggested the autotrophic cyanobacterium *Prochlorococcus spp.* as the dominant population in the near oligotrophic Subtropical Surface Water. It is likely that the second fluorescence maximum is due to the same low-light adapted ecotype. This supposition is also supported by Johnson *et al.* (1999) and Goericke *et al.* (2000). This secondary chlorophyll maximum appeared very weak in the BE area and is absent in the westernmost and northernmost areas (FR and APEI 3, respectively), in agreement with Cepeda – Moreles *et al.* (2009) who showed that the secondary chlorophyll maximum is absent from areas where the oxygenated California Current Water deepened the upper limit of the OMZ below 1% Ed490 (1% downwelling blue irradiance depth).

ACKNOWLEDGEMENTS

This material is based upon work carried out within the project **JPIO Pilot Action "Ecological aspects of deep-sea mining"**. The work has been funded by the German Federal Ministry of Education and Research (BMBF, 03F0707) under the framework of JPI Oceans. The first author would like to express sincerely thanks to the National Research and Development Institute for Marine Geology and Geoecology (GeoEcoMar) for the financial support provided for the travel and post-cruise analyses. The authors also acknowledge Dr. Pedro Martinez Arbizu, as chief scientist, Captain Mallon and the Crew of the RV SONNE for the excellent support during this cruise. We thank the financial support of the Ministry of Research, Innovation and Digitization, throughout the Programme PN III – Research of Excellence, Project PFE No. 23/30.12.2021 – AMBIACVA.

REFERENCE

Amos A.F., Roels O. A. (1977). Environmental aspects of manganese nodule mining, *Mar. Policy*, **1**: 156-163.

Barber R.T., Chavez F.P. (1983). Biological consequences of El Ninõ, *Science*, **222**: 1203-1210. http://dx.doi.org/10.1126/science.222.4629.1203

Bendschneider K., Robinson R.J. (1952). A new spectrophotometric method for the determination of nitrite in sea water, *J. Mar. Res.*, **11**: 87-96.

Billett D.S.M., Lampitt R.S., Rice A.L., Mantoura R.F.C. (1983). Seasonal sedimentation of phytoplankton to the deep sea benthos, *Nature*, **302**: 520-522. https://doi.org/10.1038/302520a0

Brandhorst W. (1959). Nitrification and denitrification in the eastern tropical north Pacific, *J. Conseil Perm. Intern. Exploration Mer,* **25**: 3-20.

Cepeda-Morales J., Godinez V.M., Gaxiola-Castro G., Beier E., Lavib M.F. (2009). Effect of the oxygen minimum zone on the second chlorophyll maximum in the Eastern Tropical Pacific off Mexico, *Cienc. Mar.*, **35**: 389-403. https://doi.org/10.7773/cm.v35i4.1622

Delcroix T., Eeldin G., Radenac M.H., Toole J., Firing E. (1992). Variation of the western equatorial Pacific Ocean, 1986-1988, *J. Geophys. Res.,* **97**(*C4*): 5423-5445.

Dore J.E., Karl D.M. (1996). Nitrite distributions and dynamics at station ALOHA, *Deep-Sea Res. Pt. II*, **43**(*23*): 385-402. https://doi.org/10.1016/0967-0645(95)00105-0

Fiedler P.C., Philbrick V., Chavez F.T. (1991). Oceanic upwelling and productivity in the eastern tropical Pacific, *Limnol. Oceanogr*, **36**(*8*): 1834-1850. https://doi.org/10.4319/lo.1991.36.8.1834

Fiedler P.C., Talley L.D. (2006). Hydrography of the eastern tropical Pacific: a review. *Prog. Oceanogr,* **69**: 143-180.

Glasby G.P. (1977). Marine manganese deposits, Elsevier Scientific Publishing Co., Amsterdam, Oxford, NY, 523 p.

Goericke R., Olson R.J., Shalapyonok A. (2000). A novel niche for *Prochlorococcus* sp. in low-light suboxic environments in the Arabian Sea and the Eastern Tropical North Pacific, *Deep-Sea Res. Pt. I*, **47**: 1183-1205. http://dx.doi.org/10.1016/S0967-0637(99)00108-9

Hanawa K., Talley L.D. (2002). Mode Waters, *In*: Siedler J., Church, J., Gloud W.J. (eds), Ocean Circulation and Climate Academic Press, London: 373-386.

Hannides A.K., Smith C.R. (2003). The northeastern Pacific abyssal plain, *In*: Black K.D., Shimmield G.B. (eds). Biochemistry of marine systems, Blackwell Science, Oxford: 208-237.

ISA (1999). Deep Seabed Polymetallic Nodule Exploration: Development of Environmental Guidelines, Proc. ISA Workshop, Sanya, China, 1-5 June 1998, The International Seabed Authority, Pub No ISA/99/02: 222-223.

Jeffrey S.W., Humphrey G.F. (1975). New spectrophotometric equations for determining chlorophylls a, b, c_1 and c_2 in higher plants, algae and natural phytoplankton, *Biochem. Physiol. Pflanz*., **167**: 191-194.

Johnson Z., Landry M., Bidigare R., Brown S., Campbell L., Gunderson J., Marra J., Trees C. (1999). Energetics and growth kinetics of a deep *Prochlorococcus spp*. population in the Arabian Sea, *Deep-Sea Res. Pt. II*, **46**: 1719-1743. https://doi.org/10.1016/S0967-0645(99)00041-7

Kessler W.S. (2006). The circulation of the eastern tropical Pacific: A review, *Prog. Oceanogr*., **69**: 181-217.

Khripounoff A., Caprais J-C., Crassous P., Etoubleau J. (2006). Geochemical and biological recovery of the disturbed seafloor in polymetallic nodule fields of the Clipperton-Clarion Fracture Zone (CCFZ) at 5,000 m depth, *Limnol. Oceanogr*., **51**(*5*): 2033-2041. https://doi.org/10.4319/lo.2006.51.5.2033

Koroleff F. (2003). Determination of phosphorus. In: Grasshoff, K., Ehrhardt, M., Kremling, K. (eds.), Methods of Seawater Analysis. 2nd edn., Verlag Chemie Gmbh, Weinheim: 125-142

Koroleff F. (1971). On the determination of reactive silicate in natural waters, *ICES CM 1971/C*, **43**.

Kuhn T., Versteegh, G.J.M., Villinger, H., Dohrmann I., Heller C., Koschinsky A., Kaul, N., Ritter S., Wegorzewski A.V., Kasten S. (2017). Widespread seawater circulation in 18-22 Ma oceanic crust: impact on heat flow and sediment geochemistry. *Geology*, **45**(*9*): 799-802. https://doi.org/10.1130/G39091.1

Lavelle J.W., Ozturgut E., Baker E.T., Swift S.A. (1972). Discharge and surface plume measurements during manganese nodule mining tests in the north equatorial pacific. *Marine Environmental Research*, **7**(*1*): 51-70. https://doi.org/10.1016/0141-1136(82)90050-2

Levin L.A. (2003). Oxygen minimum zone benthos: Adaptation and community response to hypoxia. *Oceanogr. Mar. Biol.*, **41**: 1-45.

Lukas R., Lindstrom E. (1991). The mixed layer of the Western Pacific Equatorial Pacific Ocean, *J. Geophys. Res*., **96** *Suppl*.: 3343-3357. https://doi.org/10.1029/90JC01951

Morgan C.L. (2000). Resource estimates of the Clarion-Clipperton manganese nodule deposits, *In*: Cronan D.S. (ed), Handbook of marine mineral deposits, CRC Press, Boca Raton

Morris A.W., Riley J.P. (1963). The determination of nitrate in sea water, *Anal. Chim. Acta*., **29**: 272-279.

Murphy J., Riley J. P. (1962). A modified single solution method for the determination of phosphate in natural waters, *Anal. Chim. Acta*., **27**: 31-36.

NOAA (1981). Deep Seabed Mining: Final Programmatic Environmental Impact Statement. National Oceanic and Atmospheric Administration, Washington, DC, vol. 1. https://repository.library.noaa.gov/view/noaa/30035

Odate T., Furuya K. (1998). Well-developed subsurface chlorophyll maximum near Komahashi No. 2 Seamount in the summer of 1991, *Deep-Sea Res. Pt. I*, **45**(*10*): 1595-1600.

Pennington T.J., Mahoney K.L., Kuwahara V.S., Kolber D.D., Calienes R., Chavez F.P. (2006). Primary production in the eastern tropical Pacific: a review. *Prog. Oceanogr*., **69**:285-317. https://ui.adsabs.harvard.edu/link_gateway/2006PrOce..69..285P/doi:10.1016/j.pocean.2006.03.012

Rabalais N.N., Diaz R.J., Levin L.A., Turner R.E., Gilbert D., Zhang J. (2010). Dynamics and distribution of natural and human caused hypoxia. *Biogeosciences*, **7**: 585-619.

Radziejewska T. (2002). Responses of deep-sea meiobenthic communities to sediment disturbance simulating effects of polymetallic nodule mining, *Int. Rev. Hydrobiol.,* **87**:457-477. https://doi.org/10.1002/1522-2632%28200207%2987%3A4%3C457%3A%3AAID-IROH457%3E3.0.CO%3B2-3

Radziejewska T. (2014). Characteristics of the Sub-equatorial North-Eastern Pacific Ocean's Abyss, with a Particular Reference to the Clarion-Clipperton Fracture Zone, *In*: Radziejewska T. (ed), Meiobenthos in the Sub-equatorial Pacific Abyss. A proxy in anthropogenic impact evaluation. Springer, Heidelberg: 13-28.

Reid J.L. (1973). The shallow salinity minima of the Pacific Ocean, *Deep-Sea Res*., **20**(*1*): 51-68.

Scharek R., Tupas L.M., Karl D.M. (1999). Diatom fluxes to the deep sea in the oligotrophic North Pacific gyre at Station ALOHA. *Mar. Ecol. Prog. Ser*., **182**: 55-67. https://doi.org/10.3354/MEPS182055

Schlitzer R. (2014). Ocean Data View. http://odv.awi.de

Secretariat of the Pacific Community (2016). Pacific Community 2015 Results Report. Pacific Community, Noumea, New Caledonia, ISBN: 978-982-00-1014-7.

Shinoda T., Lukas R. (1995). Lagrangian mixed layer model of the western equatorial Pacific. *J. Geophys. Res.,* **100**(*C2*): 2523-2541.

Strickland J.D.H., Parsons T.R. (1968). Determination of reactive nitrate. In: A Practical Handbook of Seawater Analysis, *Bull. Fish Res. Bd. Can*., **167**: 71-75.

Thiel H., Pfannkuche O., Schriever G., Lochte K., Gooday A.J., Hemleben C.H., Mantoura R.F.G., Turley C.M., Patching J.W., Riemann F. (1988/1989). Phytodetritus on the deep-sea floor in a central oceanic region of the northeast Atlantic. *Biol Oceanogr.,* **6**: 203-239.

Tilot V. (2006). Biodiversity and distribution of megafauna. Vol. 1: The polymetallic nodule ecosystem of the Eastern Equatorial Pacific Ocean; Vol. 2: Annotated photographic atlas of the echinoderms of the Clarion-Clipperton fracture zone. Paris, UNESCO/IOC, *IOC Technical Series*, **69**.

Tkatchenko G.G., Radziejewska T. (1998). Recovery and recolonization processes in the area disturbed by a polymetallic nodule collector simulator. *In*: Chung J.S., Olagnon M., Kim C.H. *et al.* (eds), Proceedings of 8th ISOPE Conference, vol **2**, Montreal, Canada: 282-286.

Vaccaro R.F., Ryther, J.H. (1960). Marine phytoplankton and the distribution of nitrite in the sea. *J. Conseil Perm. Intern. Exploration Mer*, **25**: 260-271.

Visbeck M., Gelpke N. (2014). World Ocean Review 3. Maribus, gGmbH, Hamburg, 163 p.

Wijesekera H.W., Rudnick D.L., Paulson C.A., Pierce S.D., Pegau W.S., Mickett J., Gregg M.C. (2005). Upper ocean heat and freshwater budgets in the eastern Pacific warm pool. *J. Geophys Res*, **110**. https://doi.org/10.1029/2004JC002511

Wilson G.D.F., Hessler R. (1987). The effects of manganese nodule test mining on the benthic fauna in the North Equatorial Pacific. *In*: Speiss F.N *et al.* (eds.) Environmental Effects of Deep Sea Dredging, SIO Reference Number 87-5, La Jolla, CA, Scripps Institution of Oceanography: 2486.

Wyrtki K. (1966). Oceanography of the eastern equatorial Pacific Oceanic. *Oceanogr. Mar. Biol. – An Annual Review*, **4**: 33-68.

Wyrtki K. (1967). Circulation and water masses in the eastern equatorial Pacific Ocean. *Int. J. Oceanol. Limnol*., **1**: 117-147.

Xie S.P., Xu H., Kessler W.S., Nonaka M. (2005). Air-sea interaction over the eastern Pacific warm pool: gap winds, thermocline dome, and atmospheric convection. *J Climate*, **18**: 5-20. https://doi.org/10.1175/JCLI-3249.1

You Y. (2003). The pathway and circulation of North Pacific Intermediate Water. *Geophys. Res. Lett*., **30**(*24*): 2291. https://doi.org/10.1029/2003GL018561

Zheng Y., van Geen A., Anderson R.F., Gardner J.V., Dean W.E. (2000). Intensification of northeast Pacific oxygen minimum zone during the Bolling-Allerod warm period, *Paleoceanography*, **15**(*5*): 528-536. https://doi.org/10.1029/1999PA0004732000